Available online at www.sciencedirect.com
SCIENCE DIRECT®
Composites Science and Technology 65 (2005) 1941–1947
COMPOSITES SCIENCE AND TECHNOLOGY
www.elsevier.com/locate/compscitech

Strain rate effect on in-plane shear strength of unidirectional polymeric composites

Jia-Lin Tsai [a], C.T. Sun [b,*]

[a] Department of Mechanical Engineering, National Chiao Tung University, Hsinchu 300, Taiwan
[b] School of Aeronautics and Astronautics, Purdue University, Grissom Hall, Room 325, West Lafayette, IN 47907 2023, United States

Received 5 July 2004; received in revised form 14 January 2005; accepted 18 January 2005
Available online 3 June 2005

Abstract

The strain rate effect on the in-plane shear strength of unidirectional composites was investigated. Off-axis S2/8552 glass epoxy block specimens were employed to produce in-plane shear failure. In order to determine the strain rate effect, specimens were tested in compression at various strain rates. For strain rates less than 1/s, experiments were conducted on an MTS machine. For higher strain rates, they were performed using a Hopkinson pressure bar. Experimental observations indicated that, for composite specimens with off-axis angles less than 10°, fiber microbuckling is the dominant failure mechanism. However, for the specimens with off-axis angles between 15° and 45°, in-plane sharing is the major failure mode. If the off-axis angle is greater than 45°, out of plane shear failure would take place. Only the in-plane shear failure mechanism was concerned in this study. The shear strain rate was obtained from the uniaxial strain rate by relating the effective plastic strain rate to the plastic shear strain rate with the aid of a viscoplasticity model. Through coordinate transformation law, the uniaxial failure stresses were then converted to a plot of shear stress versus transverse normal stress from which the shear strength in the absence of transverse normal stress ($\sigma_{22} = 0$) was obtained. Experimental results showed that the shear strength of the composite is quite sensitive to strain rate and the shear strength increases as strain rate increases. In contrast, the shear failure strain decreases as strain rate increases.

Keywords: In-plane shear strength; Strain rate; Polymeric composites; Shear stress; Transverse normal stress

1. Introduction

Unidirectional composites generally exhibit lower in-plane shear strength than longitudinal tensile and compressive strengths. This behavior is attributed to the fact that in-plane shear deformation and failure are controlled by the matrix of the composite. For polymeric composites, this indicates that the shear stiffness and strength may be sensitive to loading rate.

The quasi-static shear strength of composites has been investigated experimentally using the Iosipescu shear test [1] and a 10° off-axis tensile test [2]. In both experimental methods, in addition to shear stresses, transverse normal stresses are also present in the specimen, which may influence the value of the shear strength [3]. In order to obtain the pure shear strength, the effect of transverse normal stress must be accounted for in the data analysis. On the other hand, the rate effect on the interlaminar shear strength of carbon/epoxy composites has been studied by many authors. Bouette et al. [4] used a simple lap shear specimen and tested for the shear strength at strain rates in the range of 10^{-3}–10^{3}/s. Although the lap shear specimen was designed with the aid of FEA to reduce stress concentrations in the specimen, significant tensile peel stresses were still present. In [4], no influence of strain rate on the interlaminar

* Corresponding author. Tel.: +1 765 494 5130; fax: +1 765 494 0307.
E-mail address: sun@ecn.purdue.edu (C.T. Sun).

0266-3538/$ - see front matter © 2005 Elsevier Ltd. All rights reserved.
doi:10.1016/j.compscitech.2005.01.013

shear strength of the composite was observed. Dong et al. [5] proposed the design of a single lap specimen to estimate the interlaminar shear strength of composites under quasi-static and dynamic loadings. Both carbon/epoxy and carbon/PEEK composite specimens were tested. Experimental results showed that the interlaminar shear strength was not appreciably affected by strain rate. Ishiguro et al. [6] investigated the rate effect on unidirectional carbon/carbon composites using a double-notched lap shear specimen and found that the shear strength was influenced slightly by strain rate.

In this study, the effect of strain rate on the in-plane shear strength of a unidirectionally reinforced polymeric composite was investigated by testing off-axis block composite specimens at various strain rates. The failure mechanism was examined and the failure load associated with the in-plane shear failure was determined. A viscoplasticity model was used to help deduce the pure in-plane shear strength and to assess its sensitivity to strain rate.

2. Experimental procedures

2.1. Low strain rate test

With the presence of significant in-plane shear stresses, off-axis specimens subjected to a unaxial loading are suitable for producing in-plane shear failure. To be consistent with the high strain rate testing using the split Hopkinson pressure bar (SHPB), off-axis block specimens with the dimensions of $10 \times 6 \times 6$ mm were employed also for low strain rate testing. The block specimens were cut from a 75-ply unidirectional S2/8552 glass epoxy laminate using a diamond wheel. The fiber orientations included 15°, 30°, 45° and 60° with respect to the loading direction (10-mm direction). The specimens were lapped on a lapping machine with a 6-μm abrasive slurry to ensure smooth and flat loading surfaces. During the test, the contact surfaces of the specimen were lubricated to reduce friction.

Off-axis specimens were tested to failure on a servo-hydraulic MTS machine. A self-adjusting device as shown in Fig. 1 was adopted to eliminate potential bending moments and also to ensure the specimen to be in full contact with the loading fixtures. Three different nominal strain rates of 10^{-4}/s, 10^{-2}/s and 1/s were performed using the stroke control mode. The nominal axial strain rate was the stroke rate of the loading frame divided by the original specimen length. The corresponding true strain rate was measured by using strain gages directly mounted on the specimen. The applied load, displacement and gage signals for each test were recorded using LabView. Fig. 2 shows the nominal strain curve and the true strain curve for a 45° specimen tested at the nominal strain rate of 0.01/s. It is noted

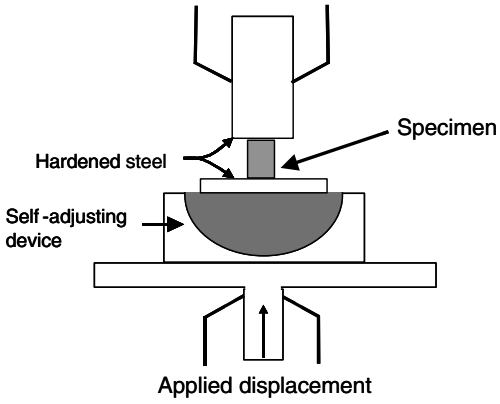

Fig. 1. Low strain rate compression test for block specimens.

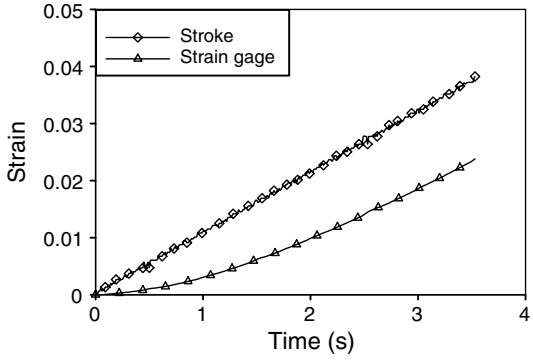

Fig. 2. Strain histories obtained from stroke and strain gage for a 45° specimen at the nominal strain rate of 0.01/s.

that the true strain is quite different from the nominal strain and, thus, the true strain rate is also different from the nominal strain rate. This discrepancy could be attributed to the use of the self-adjusting device shown in Fig. 1 in the compression test. In this study, the true strain curve was adopted for the calculation of the axial strain rate. The elastic moduli of the S2/8552 glass/epoxy composite are $E_1 = 50$ GPa, $E_2 = 20$ GPa, $G_{12} = 6.9$ GPa and $\nu_{12} = 0.3$.

2.2. High strain rate test

High strain rate experiments were conducted using a split Hopkinson pressure bar (SHPB), a simple and effective device for dynamic tests. Fig. 3 shows the schematic of a conventional SHPB setup made of hardened steel bars with 12.7 mm in diameter. The striker bar had

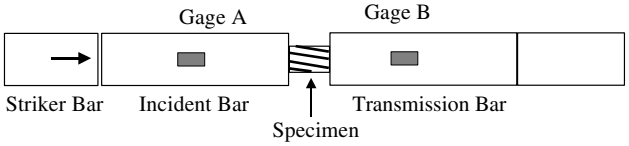

Fig. 3. Schematic of split Hopkinson pressure bar.

a length of about 101 mm, and the incident bar and the transmission bar were 910- and 550-mm long, respectively. The off-axis block specimens employed for SHPB tests were the same as those used in low strain rate tests. During the test, the block specimen was sandwiched between the incident bar and the transmission bar. It is noted that shear-extension coupling takes place in off-axis specimens under axial loading. This behavior combined with bar-specimen interfacial friction could give rise to inhomogeneous deformation in the specimen, resulting in deviations from the conventional Hopkinson bar assumption.

In order to reduce the interfacial friction, all test specimens were lapped and lubricated as suggested by Ninan et al. [7]. A pulse shaper was used to produce a gently rising loading pulse which would help in extracting reliable stress–strain curves from SHPB tests [7]. This pulse shaping can be achieved using a piece of soft material inserted between the striker bar and the incident bar. A copper tab 1.7-mm thick was used as the pulse shaper in the present study. A pair of diametrically opposite gages (gage A) as shown in Fig. 3 were mounted on the incident bar to measure both the incident and reflected signals. In the transmission bar, strain gages (gage B) were mounted at about 160-mm from the bar/specimen interface to measure the transmitted pulse. The strain gages on the bars were connected to Wheatstone circuits and then amplified using a Tektronix AM 502 amplifier. The signals were recorded using an oscilloscope at sampling rate 10 MHz. Based on one-dimensional wave propagation theory, the contact stress P_1 between the incident bar and the specimen, and P_2, the contact stress between the specimen and the transmission bar, can be extracted from the recorded signals [8]. Fig. 4 shows contact stresses P_1 and P_2 for the 30° specimen in the SHPB test. It can be seen that the peak values of the P_1 and P_2 curves are nearly the same. The average of the peak values was taken as the failure stress of the specimen in the SHPB test.

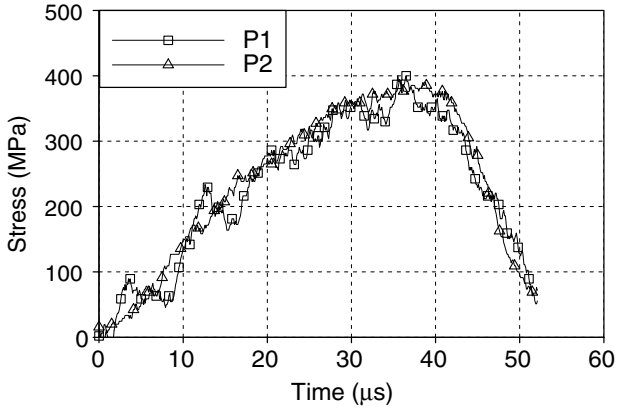

Fig. 4. Time histories of contact forces in 30° off-axis specimen.

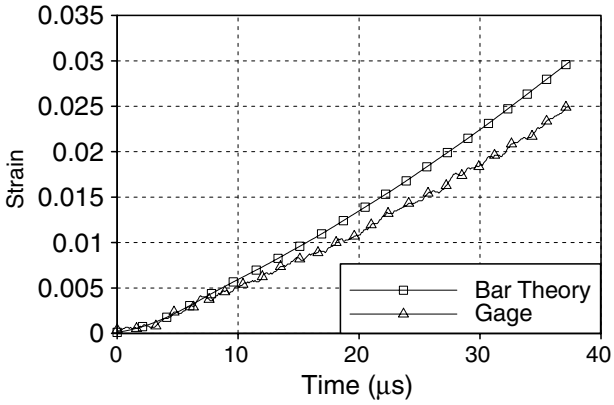

Fig. 5. Strain histories obtained from Hopkinson bar formula and strain gages, respectively, for a 30° off-axis specimen in SHPB test.

Theoretically, the strain history of the specimen during loading can be calculated using a well known Hopkinson bar formula with expressions of displacements at the ends of the bars derived from the strain responses recorded at gage A and gage B [8]. In the present study, the strain response of the specimen was also measured using a strain gage directly mounted on the specimen. Fig. 5 shows the comparison of the strain histories for the 30° specimen obtained using the Hopkinson bar formula and the strain gage on the specimen, respectively. It is evident that the strain history calculated based on the Hopkinson bar theory deviates from that directly measured on the specimen. Consequently, the respective strain rates obtained were also different. In this study, the strain rate measured directly from the specimen was used. The average axial strain rate in the SHPB tests was around 600/s.

3. In-plane shear strain rate

In the off-axis test, the strain rate was measured in terms of the total strain in the loading direction. To characterize the strain rate effect on the shear strength, the rate of shear strain should be used. In view of the foregoing, the shear strain rate should be extracted from the uniaxial compression test.

For small deformations, the total strain rate can be decomposed into elastic and inelastic parts as

$$\dot{\varepsilon}_{ij} = \dot{\varepsilon}^{\mathrm{e}}_{ij} + \dot{\varepsilon}^{\mathrm{p}}_{ij}. \tag{1}$$

The one-parameter plastic potential function,

$$f = \tfrac{1}{2}(\sigma_{22}^2 + 2a_{66}\sigma_{12}^2), \tag{2}$$

proposed by Sun and Chen [9] for modeling static nonlinear behavior of composites is employed to derive the viscoplasticity model. In Eq. (2), a_{66} is an orthotropy coefficient, and σ_{ij} are stress components referenced to the material principal directions.

Define the effective stress as

$$\bar{\sigma} = \sqrt{3f} = \sqrt{\tfrac{3}{2}}\left(\sigma_{22}^2 + 2a_{66}\sigma_{12}^2\right)^{1/2}. \tag{3}$$

With this definition of $\bar{\sigma}$ and through the equivalence of plastic work rate,

$$\dot{w}^{\mathrm{p}} = \sigma_{ij}\dot{\varepsilon}_{ij}^{\mathrm{p}} = \bar{\sigma}\dot{\bar{\varepsilon}}^{\mathrm{p}}, \tag{4}$$

the effective plastic strain rate is obtained as [10]

$$\dot{\bar{\varepsilon}}^{\mathrm{p}} = \sqrt{\frac{2}{3}}\left[\left(\dot{\varepsilon}_{22}^{\mathrm{p}}\right)^2 + \frac{1}{2a_{66}}\left(\dot{\gamma}_{12}^{\mathrm{p}}\right)^2\right]^{1/2}, \tag{5}$$

where $\dot{\varepsilon}_{ij}^{\mathrm{p}}$ are the plastic strain rate components in the material principal directions. It is noted that the effective plastic strain rate consists of two parts, i.e., the plastic normal strain rate $\dot{\varepsilon}_{22}^{\mathrm{p}}$ and the plastic shear strain rate $\dot{\gamma}_{12}^{\mathrm{p}}$. By using the one-parameter plastic potential given in Eq. (2) to describe the flow rule, these two strain rates can be expressed in terms of the normal stress and shear stress, respectively, as

$$\dot{\varepsilon}_{22}^{\mathrm{p}} = \sigma_{22}\dot{\lambda} \tag{6}$$

$$\dot{\gamma}_{12}^{\mathrm{p}} = 2a_{66}\sigma_{12}\dot{\lambda} \tag{7}$$

where $\dot{\lambda}$ is a proportionality factor and the value of a_{66} in the one parameter plastic potential for the S2/8552 glass/epoxy composite was found to be 6.0 [11]. For off-axis specimens subjected to uniaxial loading, the associated shear stress σ_{12} and transverse normal stress σ_{22} are proportional and are related via the off-axis angle. As a result, the relation between the plastic normal strain rate $\dot{\varepsilon}_{22}^{\mathrm{p}}$ and the plastic shear strain rate $\dot{\gamma}_{12}^{\mathrm{p}}$ can be obtained from Eqs. (6) and (7) as

$$\dot{\varepsilon}_{22}^{\mathrm{p}} = -\frac{-\sin\theta}{2a_{66}\cos\theta}\dot{\gamma}_{12}^{\mathrm{p}}, \tag{8}$$

where θ is the off-axis angle between the fiber orientation and the loading direction. By substituting Eq. (8) in Eq. (5), the plastic shear strain rate is expressed in terms of effective plastic strain rate as

$$\dot{\gamma}_{12}^{\mathrm{p}} = \frac{\dot{\bar{\varepsilon}}^{\mathrm{p}}}{\sqrt{\frac{2}{3}}\left[\frac{1}{2a_{66}} + \frac{\sin^2\theta}{4a_{66}^2\cos^2\theta}\right]^{1/2}}. \tag{9}$$

For off-axis specimens under monotonic uniaxial loading, the effective plastic strain rate can be determined from the axial plastic strain rate $\dot{\varepsilon}_x^{\mathrm{p}}$ as [10]

$$\dot{\bar{\varepsilon}}^{\mathrm{p}} = \frac{\dot{\varepsilon}_x^{\mathrm{p}}}{h(\theta)}, \tag{10}$$

where $h(\theta)$ is an off-axis parameter defined as

$$h(\theta) = \sqrt{\tfrac{3}{2}}\left[\sin^4\theta + 2a_{66}\sin^2\theta\cos^2\theta\right]^{1/2}. \tag{11}$$

It is noted that the axial plastic strain rate $\dot{\varepsilon}_x^{\mathrm{p}}$ can be obtained by subtracting the elastic part from the measured total axial strain rate $\dot{\varepsilon}_x$.

The total shear strain rate is obtained as

$$\dot{\gamma}_{12} = \dot{\gamma}_{12}^{\mathrm{e}} + \dot{\gamma}_{12}^{\mathrm{p}} = \frac{\dot{\sigma}_x \sin\theta\cos\theta}{G_{12}} + \dot{\gamma}_{12}^{\mathrm{p}}, \tag{12}$$

where G_{12} is the in-plane shear modulus. In view of Eq. (12) together with Eqs. (9) and (10), the total shear strain rate can be obtained from experimentally determined uniaxial stress σ_x and plastic strain $\varepsilon_x^{\mathrm{p}}$ histories. Moreover, the corresponding shear strain γ_{12} induced during the loading process can also be calculated through an incremental integration procedure.

Fig. 6 shows the time histories of effective plastic strain for the 30° and 45° specimens, respectively, corresponding to nominal axial strain rate 0.01/s. It is noted that the effective plastic strain curves were constructed based on the strain measured directly on the specimen. The plastic strain for an off-axis specimen was obtained by removing the elastic part from the total strain. Subsequently, by using Eq. (10), the corresponding effective plastic strain was obtained. In this manner, the effective plastic strain curves in Fig. 6 were generated. Note that the curves associated with different off-axis specimens are somewhat different. By taking the time derivative of the final portion of the curve, the effective plastic strain rate at the instance of shearing failure was obtained. For strain rates greater than 1/s, the effective plastic strain curves (Fig. 6) as well as the stress curves (Fig. 4) are not smooth and it is quite difficult to take the time derivative directly from the experimental data. Instead, cubic polynomials were employed to curve-fit the experimental data and then the corresponding effective plastic strain rate and the axial stress rate $\dot{\sigma}_x$ were computed from these polynomial functions. With Eqs. (9) and (12), the shear strain rates for the off-axis specimens were calculated and the results are summarized in Table 1. It is noted that the estimated shear strain rates for the specimens with various fiber orientations are somewhat different. The shear strain rates listed in Table 2 are the average values of the individual shear strain

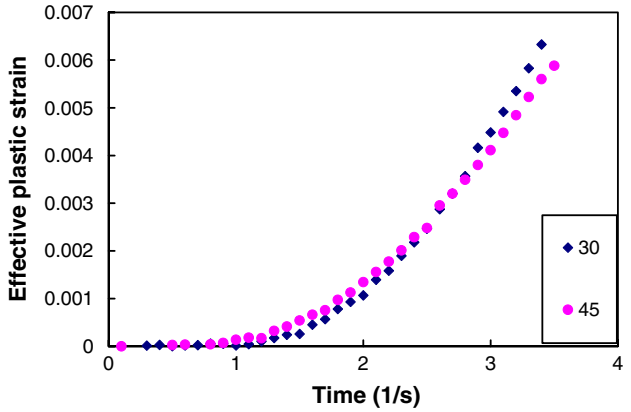

Fig. 6. Effective plastic strain histories for 30° and 45° specimens at nominal (stroke) axial strain rate 0.01/s.

Table 1
Shear strain rates obtained from the off-axis specimens subjected to axial loading

Nominal axial strain rate (1/s)	Shear strain rate (1/s)		
	15°	30°	45°
0.0001		0.000245	0.000212
0.01		0.0238	0.0176
1	1.05	2.25	1.76
600	1098	1148	802

Table 2
Pure shear strengths corresponding to different shear strain rates

Pure shear strength (MPa)	Nominal axial strain rate (1/s)	Shear strain rate (1/s)
91	0.0001	0.00023
104	0.01	0.02
114	1	1.68
137	600	1016

rates obtained from different off-axis specimens tested with the same nominal axial strain rate.

4. In-plane shear strength

Off-axis specimens tested at different loading rates were examined using an optical microscope to determine the failure mechanism. It was found that, for the 30° and 45° specimens, in-plane shearing is the failure mode within the tested strain rates. Fig. 7 shows the in-plane shearing failure in a 30° off-axis specimen. For the 15° specimen, at strain rates above 1/s, the failure mechanism was still in-plane shearing. However, at lower strain rates, it failed in fiber microbuckling. This phenomenon indicates that the fiber microbuckling load and shear failure load in the 15° specimen must be very close. The fiber microbuckling loads for off-axis specimens at various strain rates were investigated by the present authors using a microbuckling model [12]. For off-axis specimens with off-axis angles greater than 45°, out of plane shear failure occurred. In this study, the failure stress associated with in-plane shearing was considered.

Fig. 7. Shear failure mechanism for 30° specimen.

For off-axis specimens subjected to uniaxial loading, the in-plane shear stress σ_{12} is always accompanied by the transverse normal stress σ_{22}. Through the coordinate transformation law, the applied axial stress σ_x at the incipient of failure can be decomposed into transverse normal stress and shear stress in the principal material directions as

$$\begin{aligned}\sigma_{22} &= \sigma_x \sin^2(\theta+\gamma_{12}),\\ \sigma_{12} &= -\sigma_x \sin(\theta+\gamma_{12})\cos(\theta+\gamma_{12}),\end{aligned} \tag{13}$$

where θ and γ_{12} denotes the initial off-axis angle and the induced in-plane shear strain, respectively. The induced shear strain γ_{12} is calculated from Eq. (12) using an incremental integration procedure with the experimentally measured load and axial plastic strain histories. As a result, the state of failure can be expressed in terms of the combination of σ_{12} and σ_{22} as shown in Fig. 8. The result of Fig. 8 can be regarded as the in-plane shear strength of the composite in the presence of transverse normal stresses. It is important to note that, in Fig. 8, σ_{22} represents compressive stress. It is noted that the transverse normal stress has no significant effect on the failure shear stress except for high strain rates and that the effect of transverse normal stress on the in-plane shear strength seems to be weakly proportional to the compressive stress σ_{22}. A linear function appears to fit

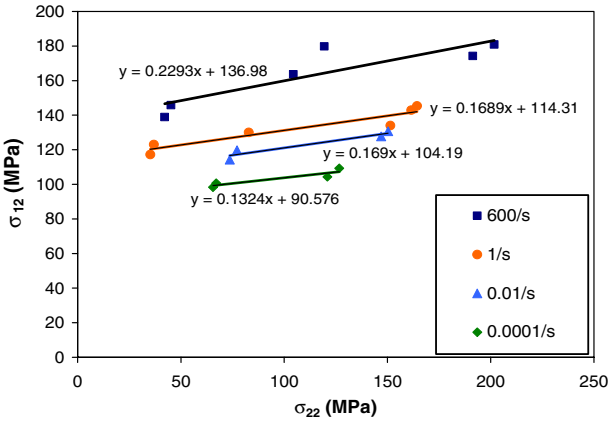

Fig. 8. Effect of compressive transverse normal stress on shear strength for different nominal axial strain rates.

the experimental data well as shown in Fig. 8 from which the pure in-plane shear strength can be obtained by extending the straight line for each strain rate to the point of $\sigma_{22} = 0$. The pure shear strengths thus obtained and the corresponding shear strain rates are listed in Table 1.

5. Results

The pure in-plane shear strengths listed in Table 1 for four different nominal axial strain rates are plotted versus the shear strain rate $\dot{\gamma}_{12}$ in Fig. 9. It is seen that the shear strength of the composite is quite sensitive to strain rate and it increases as the strain rate increases. A semi-logarithmic function,

$$S = 90.2 + 6.8 \log\left(\frac{\dot{\gamma}_{12}}{\dot{\gamma}^s_{12}}\right), \tag{14}$$

is employed to characterize the rate dependent behavior. In Eq. (14), S indicates the in-plane shear strength, and $\dot{\gamma}^s_{12}$ is the quasi-static shear strain rate which is equal to 0.00023 1/s. It is interesting to note that, on the semi-logarithmic plot, the dependence of shear strength on shear strain rate appears to be linear. By use of a non-linear rate-dependent constitutive model [11], the failure shear strains corresponding to the failure shear stresses for different strain rates were calculated. Fig. 10 shows the plot of failure shear strain versus shear strain rate. Using a semi-logarithmic function again, the rate sensitivity of failure shear strain in terms of shear strain rate can be described as

$$E = 0.042 - 0.0018 \log\left(\frac{\dot{\gamma}_{12}}{\dot{\gamma}^s_{12}}\right) \tag{15}$$

where E denotes the failure shear strain. The result indicates that the failure shear strain decreases as shear strain rate increases, which is opposite to the trend of shear strength. Similar behavior has been also observed in other polymeric composites [13,14].

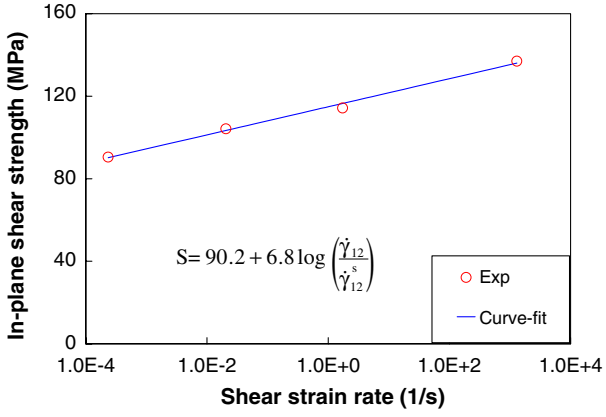

Fig. 9. Shear failure stress verses shear strain rate (S indicates the in-plane shear strength).

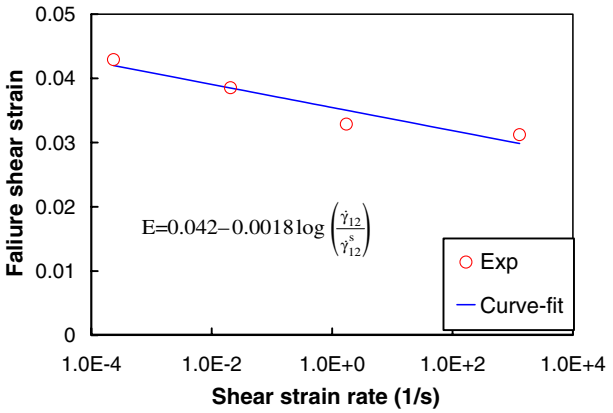

Fig. 10. Shear failure strain versus shear strain rate (E indicates the failure shear strain).

6. Summary

It has been demonstrated that off-axis block specimens of unidirectional S2/8552 glass epoxy can be used to produce in-plane shear failure at various strain rates. Experimental results indicated that in-plane shearing was the dominant failure mode for 30° and 45° specimens at axial strain rates up to 600 1/s. The effect of the transverse normal stress on the in-plane shear strength of the unidirectional composite appears to be insignificant. With the aid of a viscoplasticity model for the composite, the in-plane shear strain rate was deduced from the axial strain rate by relating the plastic shear strain rate to the effective plastic strain rate. Experimental data revealed that the in-plane shear strength increases when strain rate increases. On the other hand, shear failure strain decreases as shear strain rate increases. The failure shear strain can be expressed as a linear semi-logarithmic function in terms of a normalized shear strain rate.

Acknowledgment

This work was supported by the Office of Naval Research through Grant No. N00014-96-1-0822 to Purdue University.

References

[1] Walrath DE, Adams DF. The iosipescu shear test as applied to composite materials. Exp Mech 1983;23:105–10.
[2] Pierron F, Vautrin A. The 10° off-axis tensile test: a critical approach. Compos Sci Technol 1996;56:483–8.

[3] Pierron F, Vautrin A. Measurement of the in-plane shear strength of unidirectional composites. J Compos Mater 1997;31:889–895.
[4] Bouette B, Cazeneuve C, Oytana C. Effect of strain rate on interlaminar shear properties of carbon/epoxy composites. Compos Sci Technol 1992;45:313–21.
[5] Dong L, Harding J. A single-lap shear specimen for determining the effect of strain rate on the interlaminar shear strength of carbon fiber-reinforced laminates. Composites 1994;25:129–38.
[6] Ishiguro Y, Akatsu T, Tanabe Y, Yasuda E. Strain rate dependence on the shear strength of unidirectional carbon/carbon composites. Key Eng Mater 1999;166:139–42.
[7] Ninan L, Tsai J, Sun CT. Use of split Hopkinson pressure bar for testing off-axis composites. Int J Impact Eng 2001;25:291–313.
[8] Graff KF. Wave motion in elastic solids. New York: Dover Publications; 1975.
[9] Sun CT, Chen JL. A simple flow rule for characterizing non-linear behavior of fiber composites. J Compos Mater 1989;23(10):1009–20.
[10] Thiruppukuzhi SV, Sun CT. Model for the strain rate-dependent behavior of polymer composites. Compos Sci Technol 2001;61:1–12.
[11] Tsai J, Sun CT. Constitutive model for high strain rate response of polymeric composites. Compos Sci Technol 2002;62:1289–97.
[12] Tsai J, Sun CT. Dynamic compressive strengths of polymeric composites. Int J Solids Struct 2004;41:3211–24.
[13] Vinson JR, Woldesenbet E. Fiber orientation effects on high strain rate properties of graphite/epoxy composites. J Compos Mater 2001;35:509–21.
[14] Lee WS, Shen HC. Comparisons of deformation and fracture behavior of PC/ABS blend and ABS copolymer under dynamic shear loading. Mater Sci Technol 2004;20:8–15.